International Journal of Heat and Mass Transfer 215 (2023) 124470

Contents lists available at ScienceDirect

International Journal of Heat and Mass Transfer

journal homepage: www.elsevier.com/locate/ijhmt

Influence of system pressure on flow boiling in microchannels

Vivian Y.S. Lee, Tassos G Karayiannis*

Department of Mechanical and Aerospace Engineering, Brunel University London, Kingston Lane, Uxbridge, Middlesex UK UB8 3PH

ARTICLE INFO

Article history:
Received 21 December 2022
Revised 18 June 2023
Accepted 30 June 2023

Keywords:
system pressure
microchannel
two-phase
heat transfer

ABSTRACT

The effect of pressure on the flow boiling characteristics of HFE-7200 between 1.0 to 2.0 bar was investigated in a parallel microchannel heat sink (D_h = 0.48 mm, 44 channels). The mass flux and subcooling degree were kept constant at 200 kg/m^2 s and 10 K respectively, while heat flux ranged from 26.1 – 160.7 kW/m^2. Increasing system pressure decreased the vapour density ratio, thus leading to reduced pressure drop, increased bubble generation frequency and two-phase heat transfer coefficients in the system, though this may not be apparent at low superheat degrees at higher pressures. Smaller bubble diameters were observed at higher pressures and resulted in a delay in flow regime transition to slug flow, which is prone to flow reversal. The experimental work showed promising means to manage flow instabilities and enhance heat transfer performance in two-phase microchannel systems for HFE-7200.

1. Introduction

Flow boiling characteristics in microchannels are dependent on fluid properties and operating parameters including heat flux (q"), mass flux (G), subcooling degree (ΔT) and operating pressure (P). Experimental and analytical studies on pool boiling and flow boiling have demonstrated a strong influence of system pressure on nucleation criteria, bubble growth and departure cycle by virtue of the sensitivity of the thermo-physical properties of a given working fluid on system pressure [1,2]. The influence of pressure on key fluid properties (eg. vapour density and surface tension), which affect both nucleate boiling and convective boiling flow mechanisms as well as the bubble nucleation dynamics result in variations in flow regime development and flow boiling behaviour in microchannels. Generally, a reduction in microchannel two-phase pressure drop is reported at higher working pressures [3–5]. This could be due to the dependence of the frictional and momentum pressure drop components on the void fraction and flow regimes, which may be influenced by the viscosity and the liquid-vapour density ratio [6]. The critical heat flux (CHF) of boiling systems is known to be enhanced at higher pressures (provided the working pressure is less than one third of the critical pressure [7]), as demonstrated through the hydrodynamic theory by Kutateladze [8], Zuber [9] and more recently in [10]. Flow instabilities, which may lead to the CHF condition and present practical issues such as flow maldistribution and dryout in parallel channel heat sinks, may also be delayed by increasing operating pressure [3,11] without major heat sink design effort and pressure drop penalty. Several other flow instability mitigation strategies have been proposed [12,13]. These include surface modifications and use of inlet restrictors.

Clear understanding of the inter-relationship between the above-mentioned parameters (i.e. heat flux, mass flux and degree of subcooling) and operating pressure offers useful insight into optimising the performance of two-phase thermal management systems. In this study, the flow boiling characteristics of HFE-7200 at three inlet pressures (i.e. 1, 1.5 and 2 bar) was investigated in a parallel microchannel heat sink (i.e. D_h = 0.48 mm), where the degree of inlet subcooling was kept constant at 10 K.

1.1. Effect on Bubble Nucleation

Several studies have found that bubble departure frequency increases with increasing system pressure. Euh et al. [14] conducted a flow visualisation study on subcooled flow boiling of water in a 19.1 mm diameter tube at system pressures of 1.67 bar – 3.46 bar, mass fluxes of 214 – 1869 kg/m^2 s, heat flux between 61 – 238 kW/m^2 and subcooled conditions ranging from 7.5 – 23.4 K. Although the tube diameter investigated is more relevant to macroscale flow boiling, the fundamental findings on the dependency of bubble nucleation behaviour on system pressure at the macroscale level are still useful in the understanding of microscale boiling behaviour. Euh et al. [14] attributed the enhanced bubble generation frequency at higher pressures to the increase in vapour density corresponding to pressure increase. Considering the mechanical equilibrium of a vapour nucleus [6], the authors rea-

* Corresponding author.
E-mail address: Tassos.Karayiannis@brunel.ac.uk (T.G. Karayiannis).

https://doi.org/10.1016/j.ijheatmasstransfer.2023.124470

Nomenclature

$\bar{h}_{tp}$	average heat transfer coefficient [W/m^2 K]
$h_{(z)}$	local heat transfer coefficient [W/m^2 K]
D_h	hydraulic diameter [m]
G	mass flux [kg/m^{2}s]
H_{ch}	channel height [m]
k	thermal conductivity [W/m K]
L	length [m]
N	number of channels [-]
q''	heat flux [W/m^2]
r_c	cavity radius [m]
$T_{f(z)}$	local fluid temperature [°C]
$T_{w(z)}$	temperature of channel bottom wall [°C]
W	width [m]
x	vapour quality [-]
z/L	dimensionless axial location [-]
ΔP	pressure drop [kPa]

Greek letters

η	fin efficiency [-]
ρ_g	gas density [kg/m^3]

Subscripts

b	base
ch	channel
f	fin
hs	heat sink
i	inlet
ip	inlet plenum
manifold	manifold/plenum
meas	measured pressure drop
nb	nucleate boiling
pen	penalty
plain	plain microchannel
sat	saturated
sc	sudden contraction
sp	single-phase
sub	subcooled
tp	two-phase
w	wall

soned that higher vapour density resulted in lower required wall superheat for bubble nucleation, which reduced waiting time between consecutive bubble ebullition cycles and thus increased bubble generation frequency. Bubble departure frequency was also reported to increase with pressure in the work of Murshed et al. [15].

Smaller bubble departure sizes were also noted by Euh et al. [14] at higher pressures. Referring to the force balance models developed by Situ et al. [16] and Klausner et al. [17], it was noted that the higher vapour density at higher pressures also significantly lowered the drag force acting on bubbles, which reduced bubble departure diameter and bubble growth time. Flow visualisation also revealed smaller bubble diameters in Kuo and Peles [3], Prodanovic et al. [18] and Yuan et al. [19]. The latter used the liquid-vapour density ratio to correlate the pressure effect on bubble diameters. Similarly, applying the force balance model by Klausner et al. [17] and comparing bubble growth and departure time of water, ethanol, R134a and R245fa, Mahmoud and Karayiannis [2] showed that bubble growth rate exhibited a strong dependence on liquid-vapour density, surface tension and viscosity ratio of a fluid.

Furthermore, the range of active nucleation sites may also increase under higher pressure conditions. Mahmoud and Karayiannis [2] highlighted the importance of surface conditions, namely the size range of active nucleation sites for bubble nucleation and boiling incipience wall superheat on heated surfaces. The authors predicted this range using the model proposed by Hsu [1], which is a function of wall superheat condition as well as fluid properties including surface tension, vapour density and latent heat of vapourisation. The analysis revealed that the required wall superheat for nucleation in certain fluids, for instance, water, decreased drastically when system pressure was increased.

Consequently, fabricating cavities of appropriate sizes based on the nucleation theory on boiling surfaces as well as modifying system pressure to reduce the required wall superheat for nucleation could potentially mitigate flow instabilities related to explosive boiling as well as delay the occurrence of CHF in two-phase systems. Kuo and Peles [3,20] investigated the use of re-entrant cavities to supress flow instabilities and delay flow instability-induced premature CHF by promoting controlled bubble growth in the channels. Cavities 7.5 μm wide were etched on the sidewalls of the 223 μm hydraulic diameter silicon microchannels. The experimental study was conducted with water as the working fluid at base heat fluxes up to 2.5 MW/m^2, mass fluxes between 86 – 520 kg/m^2 s and exit pressures ranging from 50 – 205 kPa. High wall superheat at the inception of boiling caused vigorous flow oscillations in the channels at low operating pressures, leading to early transition to the CHF condition in the system. At higher system pressures, a stable boiling regime was established after boiling incipience and lower pressure gradient in the channels resulted in an increase in CHF. It was not explicitly stated if the degree of inlet subcooling was kept constant in the study of Kuo and Peles [3] and [20]. For subcooled flow boiling of water in tubes of diameter between 0.406 mm – 2.54 mm, Mudawar and Bowers [21] reported an increase in CHF with increase in pressure from 2.5 bar to 30 bar. CHF did not vary significantly following further increase in pressure but fell as pressures approach the critical point. Nonetheless, the degree of inlet subcooling, which could affect both wall superheat required for bubble nucleation (as noted in Mahmoud and Karayiannis [2]) and the development of CHF condition was not kept constant in the study of pressure effect by Mudawar and Bowers [21].

1.2. Effect on Heat Transfer Rates

In accordance with the findings of enhanced bubble departure frequencies presented above, many studies have found that increasing system pressure improved flow boiling heat transfer performance [22–25]. Amongst these, the influence of pressure on the latent heat of vapourisation [22], density ratio and surface tension [23] and [25] were highlighted as plausible reasons to heat transfer enhancement. Despite concluding an insignificant effect of pressure on average heat transfer coefficient in their microchannel evaporator at low mass flux in an earlier paper by Bertsch et al. [26], a slight increase in heat transfer coefficient with increase in pressure was reported at a higher mass flux condition in a later study by Bertsch et al. [27]. Agostini et al. [24] reported a significant increase in local heat transfer coefficients with increase in pressure for refrigerant R236fa, but found a negligible pressure effect on heat transfer coefficients for R245fa. The authors suggested that the less obvious pressure effect observed for R245fa could be due to the high experimental uncertainties as the experiments involving the fluid was conducted under relatively low heat fluxes. Thiangtham et al. [28] also found a slight increase in heat transfer coefficients and attributed this to higher bubble generation at higher system pressures in the channels.

On the other hand, the effect of pressure has also been found to be insignificant at vapour quality regions where nucleate boil-

ing might not be the dominant mode of heat transfer. Wen et al. [29] studied the flow boiling of R134a in serrated fin minichannels and found that increasing the system pressure from 2.9 bar to 4.5 bar improved heat transfer coefficients at low to moderate vapour qualities (vapour quality around 0.5), while the pressure effect was negligible in the high vapour quality region where convective boiling was assumed to dominate. The authors reasoned that higher bubble generation activity at higher pressures in the low vapour quality region is as a result of the reduction in latent heat of vapourisation following system pressure increase. Similar enhancement effect, i.e. limited to low vapour qualities were also reported for the flow boiling of R134a in microtubes [30,31]. Karayiannis et al. [30] reported an increase in heat transfer coefficients in a 1.1 mm diameter tube at vapour quality less than 0.3, corresponding to an increase in pressure from 6 bar to 10 bar, but found no enhancement in heat transfer coefficients at higher vapour qualities with the same increment in system pressure. The higher heat transfer coefficients in the low vapour quality region was attributed to the reduction of surface tension with increase in system pressure, which resulted in smaller bubble departure diameters in the nucleate boiling dominant region. In and Jeong [31] studied the effect of system pressure (1.58 bar and 2.08 bar) on fluid R123 in a 0.19 mm diameter tube and found no heat transfer enhancement at the higher pressure condition in the high vapour quality region, where convective boiling reportedly dominated. Note that the work did not include flow visualisation, even though the authors inferred, based on similar studies, that elongated bubbly flow dominated at high vapour qualities. They also found a stronger effect of mass flux and heat flux on heat transfer coefficients at lower pressures. It was suggested that due to the lower vapour density of R123 at lower pressures, the elongated bubbles travel at a higher velocity, causing the thickness of the surrounding liquid film to be thinner, which resulted in a higher dependence of heat transfer on mass flux and heat flux at lower pressures.

In contrast, Saisorn et al. [4] reported a significant decrease in heat transfer coefficients of R134a in a 1.75 mm diameter tube when system pressure increased from 8 bar to 10 bar. They theorised that smaller latent heat of vapourisation and lower liquid viscosity at higher pressures resulted in thinner liquid films on the tube walls, which could have a higher tendency to rupture compared to thicker liquid films, thus leading to local dryout and reduced overall heat transfer coefficients.

2. Experimental Methodology

An experimental facility was set up as part of a larger study into flow boiling behaviour in parallel microchannel systems, as shown in Fig. 1. The main flow loop with HFE-7200 is circulated using a micro gear pump and digital pump drive (GJ-N23FF2S from Micropump® and ISMATEC Reglo ZS© respectively) to the microchannel evaporator test section from the tank. The pressure in the system is controlled using an immersion heater in the reservoir. Two Coriolis mass flowmeters, the OPTIMASS 3000 S01 for mass fluxes $\leq$300 kg/m^2 s and OPTIMASS 3000 S03 for mass fluxes $>$300 kg/m^{2}s from Krohne, are used to measure flow rate in the system. The temperature at the inlet of the test section, which controls the degree of subcooling in the study is regulated using a pre-heater. Heat from the test section is rejected to the plate heat exchanger, which is cooled by the chiller system using water-glycol. A subcooler was located upstream of the gear pump in order to maintain feed temperatures within the operating range of the seals. A National Instruments Data Acquisition System (DAQ) was used to log and monitor measurements in the experiments. After steady state conditions are achieved, i.e. when the experimental variables do not change by more than $\pm$ 0.2 g/s for mass flow rates, $\pm$ 0.5 K for inlet/outlet temperature and $\pm$ 0.05 bar for the inlet/outlet pressure over a period of at least 180 s. Live flow visualisation images provided by the Phantom Miro Lab110 high-speed camera, Huvitz HSZ-645TR microscope and LED lighting system operating at 5000 frames/s and a resolution of 512$\times$512 pixels were also used to assess steady flow phenomena before data acquisition. Flow visualisation was conducted at four locations incrementally (i.e. locations 1 to 4, from inlet to outlet, see Fig. 2) along the channel length at the middle of the heat sink during each experimental run. Each dataset was acquired over a duration of 90 s at a frequency of 1 kHz and averaged for data reduction.

The test section is shown in Fig. 3 and has been described in detail in [32]. There are 44 parallel microchannels on the copper heat sink, each nominally 0.7 mm in height, 0.35 mm in width and 20 mm in length. The heating to the test section is provided by cartridge heaters, controlled by a variac as illustrated previously in Fig. 1. The temperature near the bottom of the channels (i.e. 5 mm from the bottom wall) are measured in five locations along the streamline direction as well as in the traverse direction. The heat flux is calculated using the temperature gradient measured along the height of the block. The cover plate was fabricated out of polycarbonate to provide viewing to the flow phenomenon in the channels and manifolds. The inlet and outlet pressures and temperatures are measured at the manifolds using two Omega^{TM} PXM409-007BAI pressure transducers and calibrated K-type thermocouples, see Fig. 3(a) for the locations. Additionally, the total pressure drop across the inlet and outlet manifold are measured using an Omega^{TM} PX409-015DWUI differential pressure transducer with a range up to 1 bar.

2.1. Data Reduction

The data reduction procedure has been reported in detail in [32]. The local heat transfer coefficient is calculated as follows based on temperature measurements at dimensionless locations z/L = 0.17, 0.34, 0.5, 0.67 and 0.83:

$$h_{(z)} = \frac{q_b\ (W_{ch} + W_{fin})}{\left(\ T_{w(z)}\ -\ T_{f(z)}\ \right)\ (\ W_{ch} + 2\ \eta\ H_{ch}\ )} \tag{1}$$

where W_{ch}, W_{fin} and H_{ch} are the channel width, fin thickness and channel height respectively. The fin efficiency, η and fin parameter, m, are found iteratively, see [7] and [32].

The two-phase pressure drop in the channel, $\Delta P_{tp,}$ is found by the following relation:

$$\Delta P_{tp} = \Delta P_{ch} - \Delta P_{sp} \tag{2}$$

where ΔP_{sp} is the single-phase pressure drop in the subcooled region and ΔP_{ch} is the pressure drop in the channel, given by:

$$\Delta P_{ch} = \Delta P_{meas} - \Delta P_{manifold} \tag{3}$$

ΔP_{meas} is the measured pressure drop at the inlet and outlet manifolds (see Fig. 3(a)) using the differential pressure transducer and $\Delta P_{manifold}$ is the pressure change in the manifolds. The calculation for the manifold pressure changes have previously been presented in detail in [32].

The inlet pressure, P_i, is taken as the pressure measured at the inlet manifold of the heat sink by the inlet pressure transducer. This is also referred to as the system pressure in this publication. For all other calculations, such as in the evaluation of local saturation pressures and two-phase pressure drop, the pressure at the inlet of the channel array, $P_{i,ch}$, is used. This is corrected for pressure losses in the inlet manifold:

$$P_{i,ch} = P_i - P_{ip} - P_{sc} \tag{4}$$

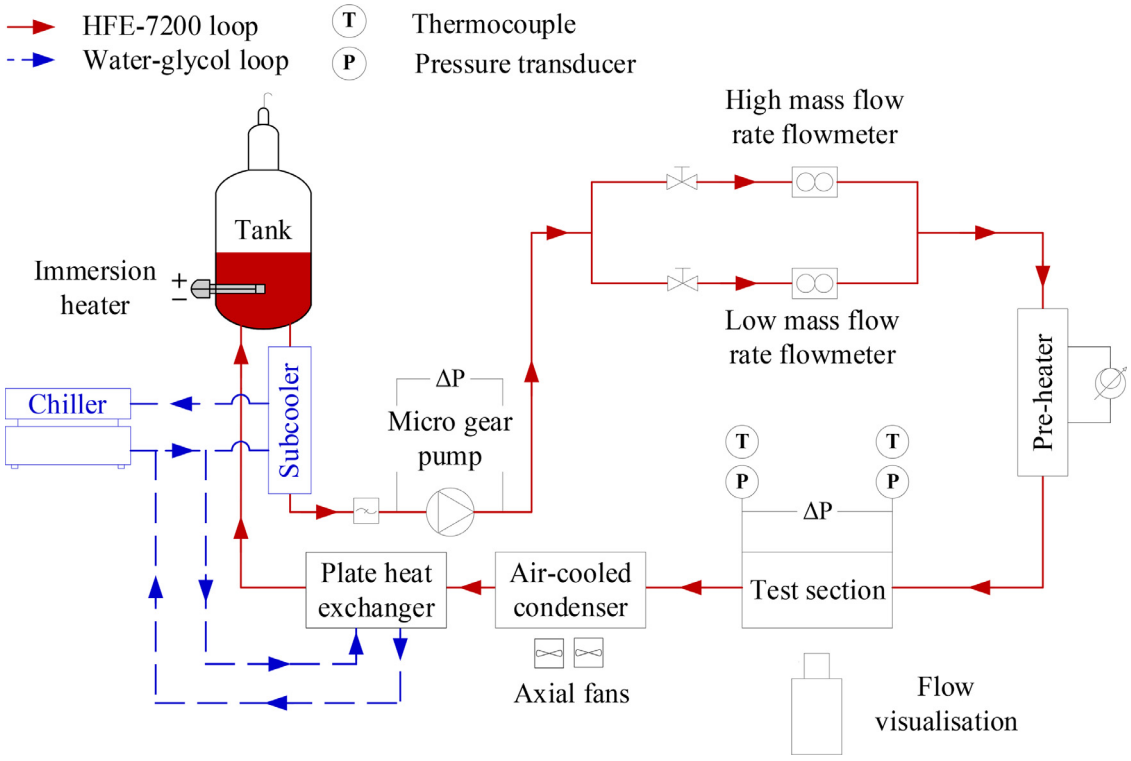

Fig. 1. Flow boiling experimental facility [32].

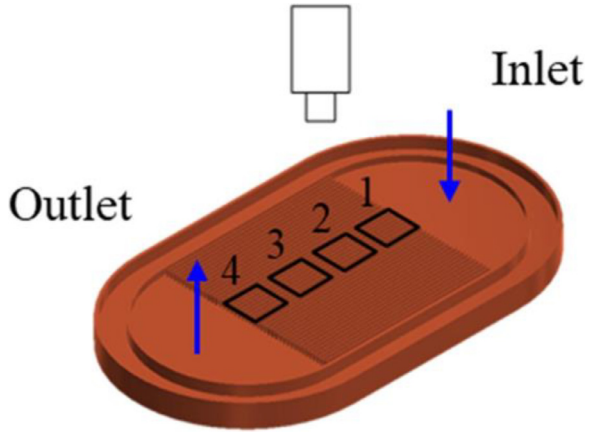

Fig. 2. Camera locations for flow visualisation, taken from [32].

where P_{ip} is the pressure drop in the inlet manifold and P_{sc} is the pressure drop due to sudden contraction into the microchannel array, see [32]. Single-phase validation was conducted to verify the experimental measurements and data reduction procedure. For a constant inlet subcooling degree of 10 K the inlet temperature at P = 1.0, 1.5 and 2.0 bar are 65°C, 79°C and 88°C respectively. The mass flux was kept consistent at 200 kg/m^2 s for wall heat fluxes ranging from 26.1 – 160.7 kW/m^2. Since the mass flux and inlet subcooling were kept constant in the experiments, the effect of pressure is isolated from effects of mass flux and inlet subcooling in this analysis. As mentioned above, details on the data reduction procedure, validation using single-phase experiments and reproducibility of our experiments are included in Lee and Karayiannis [32]. The experimental uncertainties are presented in Table 1 where the propagated uncertainties are based on the method in [33].

Table 1
Experimental uncertainties.

Equipment/Parameter	Uncertainty
K-type thermocouple	± 0.2 K
Inlet/outlet pressure transducer	± 0.08 % (full-scale)
Differential pressure transducer	± 0.25 % (full-scale)
Hydraulic diameter	± 0.38 – 0.42 %
Mass flow rate	± 0.035 %
Channel mass flux	± 0.63 %
Fanning friction factor	± 2.39 – 2.46 %
Average Nusselt number	± 5.57 – 11.71%
Channel pressure drop	± 0.1 – 0.57 %
Local heat transfer coefficient	± 3.87 – 9.67%
Local vapour quality	± 2.13 – 9.23 %
Heat flux	± 1.96 – 4.35 %

3. Results

3.1. Fluid properties and nucleation cavity size

As highlighted above, fluid property change with system pressure could have a significant effect on flow boiling characteristics in microchannels. Relevant fluid properties of the working fluid, HFE-7200, at system pressures from P = 1 bar to P = 2 bar are summarised in Table 2. Important dimensionless ratios are shown in Table 2 for the range of pressures investigated in this study.

3.1.1. Increasing system pressure from 1 bar to 1.5 bar

Corresponding to a pressure increase from 1 bar to 1.5 bar, liquid viscosity dropped by 13.9 %, while the vapour density of the fluid rose by almost 50 %. The large rise in vapour density resulted

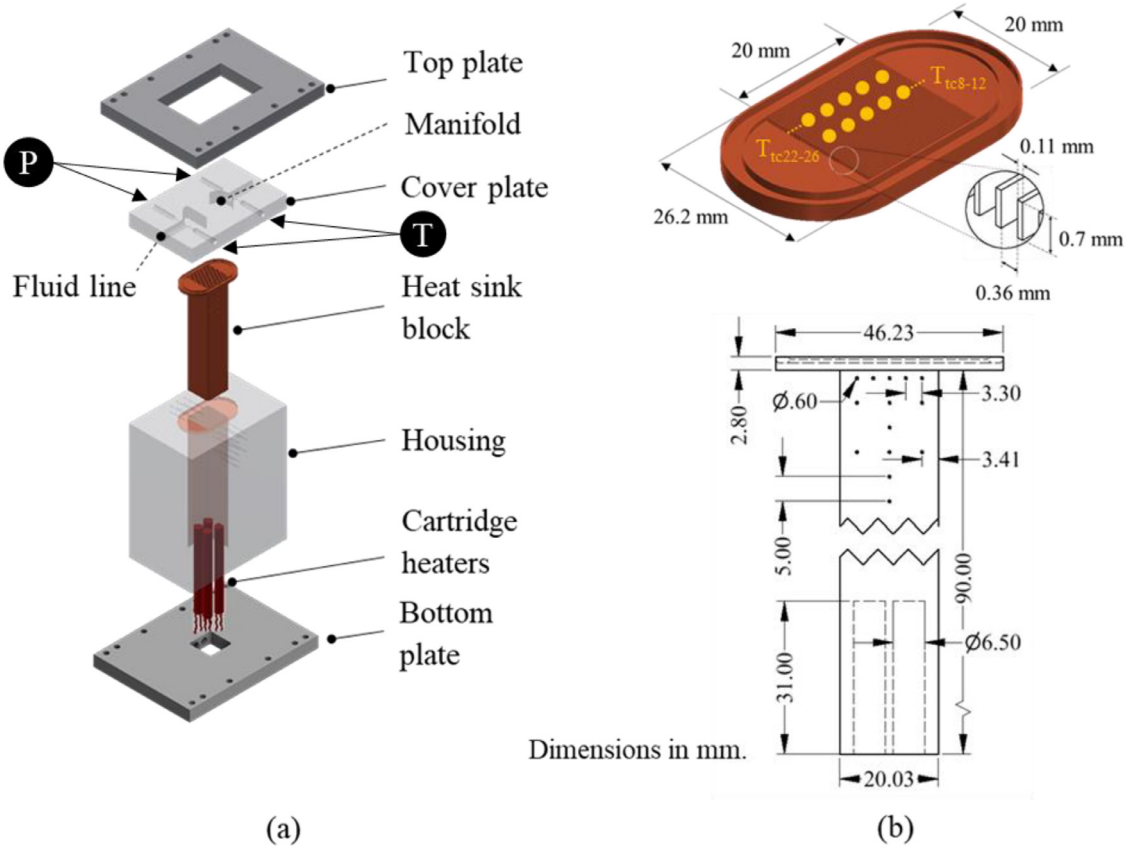

Fig. 3. Test section (a) Exploded view (b) Details of microchannel heat sink. The locations of wall temperature measurement are annotated, see also [32]. P and T indicate locations of pressure transducer ports and thermocouple locations respectively.

Table 2
Properties of fluid HFE-7200 at different system pressures.

P_{sat}[bar]	T_{sat}[°C]	c_p [J/kg K]	i_{fg} [kJ/kg]	ρ_g[kg/m^3]	μ_f[kPa s]	μ_g[kPa s]	σ[mN/m]
1.0	75.1	1086	110	9.7	0.36	0.012	9.6
1.5	88.7 (+18.1%)	1135(+4.5 %)	107(-2.7 %)	14.3(+47.4 %)	0.31(-13.9 %)	0.013(+8.3 %)	8.4(-12.5 %)
2.0	99.0(+11.6%)	1175(+3.5%)	105(-1.8%)	19.0(+32.9%)	0.27(-12.9%)	0.013-	7.5(-10.7%)

Percentage change with incremental pressure step shown in brackets.

in a 34 % fall in liquid to vapour density ratio while the reduction in liquid viscosity decreased liquid to vapour viscosity ratio by 16.8 %. Additionally, the reduced pressure ratio (i.e. $P_r = P_{sat}/P_{crit}$, where $P_{crit} = 20.1$ bar) increased significantly by 40 % as the inlet pressure was increased to 1.5 bar. Liquid density, gas viscosity, specific heat and latent heat of evaporation of HFE-7200 did not vary significantly in the range of this study (varied by less than 5 % between 1 bar and 1.5 bar).

3.1.2. Increasing system pressure from 1.5 bar to 2 bar

Between P = 1.5 bar and P = 2 bar, a proportional fall in liquid viscosity (-12.9 %) and surface tension (-10.7 %) was recorded. Vapour density varied less between operating pressures of 1.5 bar and 2 bar, and rose by only 32.9 % compared to the +47.4 % in the previous pressure increment. This contributed to a 26.1 % drop in liquid to vapour density ratio and a 14.8 % reduction in liquid to vapour viscosity ratio. The reduced pressure ratio rose moderately by 42.9 % when the pressure was increased from 1.5 bar to 2 bar. Similarly, the variation in liquid density, gas viscosity, specific heat and latent heat of evaporation were negligible with pressure increment to 2 bar.

3.1.3. Size of active nucleation sites

Additionally, based on the Hsu nucleation model [1], the size of active nucleation cavities was associated with the physical properties of the working fluid, saturation temperature and subcooling, as well as the thickness of the thermal boundary layer surrounding a nucleating bubble. The saturation temperature of the fluid is in turn influenced by the system pressure. Therefore, the relation is used to predict the active cavity size radii, r_c, for operating pressures in the range of P = 1 – 2 bar, with the assumption of zero subcooling in the system and $D_h = 475$ µm, see Fig. 4.

The range of active nucleation sites increased rapidly with superheat, especially in the low wall superheat region, namely where $0\ K < \Delta T_{sup} < 5\ K$. The largest cavity radius in the active nucleation range is around 55 µm and appeared to be insensitive to pressure change, at least within the pressure range of this study (P = 1 – 2 bar). The minimum cavity size, in contrast, varied distinctly with change in inlet pressure. This is mainly due to the notable increase in vapour density with pressure increase (see Table 2 and Table 3). For a nominal ΔT_{sup} of 10 K, minimum r_c extended from 0.11 µm to 0.08 µm with pressure increase from P = 1 bar to P = 1.5 bar, and further to 0.06 µm with respect to subsequent pressure increase to P = 2 bar.

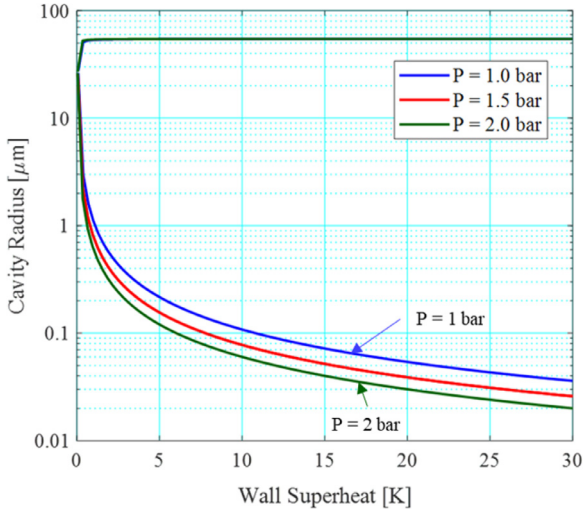

Fig. 4. Effect of system pressure on the size range of active nucleation sites using HFE-7200, based on the nucleation model by Hsu [1].

Table 3
Property ratios and dimensionless numbers of fluid HFE-7200 at different system pressures.

P_{sat} [bar]	$(\frac{\rho_f}{\rho_g})$ [-]	$(\frac{\mu_f}{\mu_g})$ [-]	P_r [-]	Ja [-]
1.0	134	29.2	0.05	17.8
1.5	88.4(-34.0 %)	24.3(-16.8 %)	0.07(+40.0 %)	9.1(-48.9 %)
2.0	65.3(-26.1 %)	20.7(-14.8 %)	0.10(+42.9 %)	5.5(-39.5 %)

Percentage change with incremental pressure step shown in brackets.

Table 4
Flow pattern transition vapour qualities at G = 200 kg/m^2 s and ΔT_{sub} = 10 K for wall heat fluxes ranging from $q_w^{"}$ = 26.1 – 161.6 kW/m^2. $X_{B\text{-}S}$: bubbly to slug; $X_{S\text{-}C}$: slug to churn; $X_{C\text{-}A}$

P[bar]	$x_{B\text{-}S}$[-]	$x_{S\text{-}C}$[-]	$x_{C\text{-}A}$[-]
1.0	0.037	0.068	0.304
1.5	0.064	0.119	0.314
2.0	0.066	0.122	0.353

In conclusion, increasing system pressure had a remarkable effect on the vapour density of fluid HFE-7200. Surface tension and liquid viscosity also fell moderately with pressure increase. Nonetheless, a smaller variation in fluid properties were observed between pressures P = 1.5 bar and P = 2 bar. The range of active nucleation sites, as predicted using Hsu's model [1], increased especially with increasing wall superheat and extended with increase in system pressure.

3.2. Flow Patterns

Flow patterns developed in a similar manner at all three investigated pressure conditions, i.e. from bubbly, slug, churn to annular flow, see Fig. 5. Generally, there was an increase in flow pattern transition vapour quality with increase in inlet pressure, as summarised in Table 4. There was notable delay in transitional boundaries between pressures P = 1.0 bar and P = 1.5 bar. For instance, transition from bubbly to slug flow occurred accordingly at x = 0.0037 at P = 1 bar, x = 0.064 at P = 1.5 bar and x = 0.066 at P = 2 bar. With pressure increase from P = 1.5 bar and P = 2 bar, there was a smaller difference in flow pattern transition vapour qualities.

Delayed transition from bubbly to slug flow could be due to smaller bubble departure diameters at higher system pressures, as illustrated in Fig. 6. The bubble diameters were measured using ImageJ in one random channel, at five separate frames sampled from the corresponding high-speed video. Fig. 7 to Fig. 9 show the distribution of bubble diameters observed in the bubbly flow regime at $q_w^{"} \sim 50$ kW/m^2 for inlet pressure conditions of 1 bar, 1.5 bar and 2 bar respectively.

Bubble size was observed to decrease with increasing system pressure, as evidenced by the shift in distribution peak to lower bubble diameters at higher operating pressures. The median bubble diameter calculated from each distribution decreased from 98.5 μm to 82 μm between P = 1 bar and P = 1.5 bar, i.e. a percentage difference of 16.8 %, and at P = 2 bar decreased further to 67 μm (by 18.3 %). Smaller bubbles have a smaller tendency to coalesce in the channels, which may explain the delay in transition from bubbly to slug flow at higher system pressures. Smaller bubble sizes at higher operating pressure conditions were similarly observed by Euh et al. [14], Prodanovic et al. [18] and Yuan et al. [19] in macrotubes, as well as Kuo and Peles [3] for parallel microchannels.

Amongst these studies, Euh et al. [14] cited the change in vapour density with system pressure increase as the main reason for the reduction in bubble departure diameter. The reduction in liquid-vapour density ratio, $(\frac{\rho_f}{\rho_g})$, with pressure increase was also cited as a physical property that controlled bubble departure diameters in flow boiling by Prodanovic [18]. Accordingly, $(\frac{\rho_f}{\rho_g})$ decreased by 34 % and 26.1 % with pressure increase to P = 1.5 bar and P = 2 bar respectively. Vapour density has also been cited as an important parameter in bubble nucleation dynamics [2,3,14], especially in the force balance models developed by Situ et al. [16] and Klausner et al. [17] to estimate flow boiling bubble departure diameter. The drag force acting on a nucleating bubble, both in the streamwise direction as well as the direction normal to the flow, is a function of bubble growth rate [2], which is estimated based on the correlation by Zuber [34] in the model of Situ et al. [16], and using the model developed by Mikic et al. [35] in Klausner's drag equation. Zuber's correlation is given as follows [34]:

$$\dot{r}_b = \frac{1}{2\sqrt{t}} \frac{2\ b\ Ja\ \sqrt{\alpha_f}}{\sqrt{\pi}} \tag{5}$$

where b is a constant between 1 and $\sqrt{3}$ and α_f is the liquid thermal diffusivity. The Jakob number, Ja, is defined as follows:

$$Ja = \frac{\rho_f\ c_{p,f}\ (T_w - T_{sat})}{\rho_g\ i_{fg}} \tag{6}$$

On the other hand, the model developed by Mikic et al. [35] is given below:

$$\dot{r}_b = \frac{1}{2\sqrt{t}} \sqrt{\frac{12\ \alpha_f}{\pi}}\ Ja \left(1 - \frac{T_v - T_{sat}}{T_w - T_{sat}}\right) \tag{7}$$

Evidently, bubble growth rate is a function of Ja, which represents the ratio of sensible heat to latent heat absorbed during phase change. As mentioned above, liquid density, specific heat and latent heat of vapourisation did not vary significantly with pressure, at least in the range of this study. The notable increase in vapour density, namely by 47.4 % at P = 1.5 bar and 32.9 % at P = 2 bar, result in reductions in Ja by 48.9 % and 39.5 % respectively. The smaller Jakob number drastically reduces the drag force acting on a bubble growing from a nucleation site. Since less drag force is imposed on the bubble, the force balance equations are more easily overcome in the direction of the flow, thus resulting in smaller bubble departure diameters and bubble sizes in the channels at higher inlet pressures.

Lee [36] concluded that in addition to the drag force on a bubble, surface tension forces are also dominant forces controlling bubble departure diameter. Surface tension dropped by 12.5 % between P = 1 bar and P = 1.5 bar, and by a further 10.7 % with pressure increase to P = 2 bar. The resultant lower surface tension

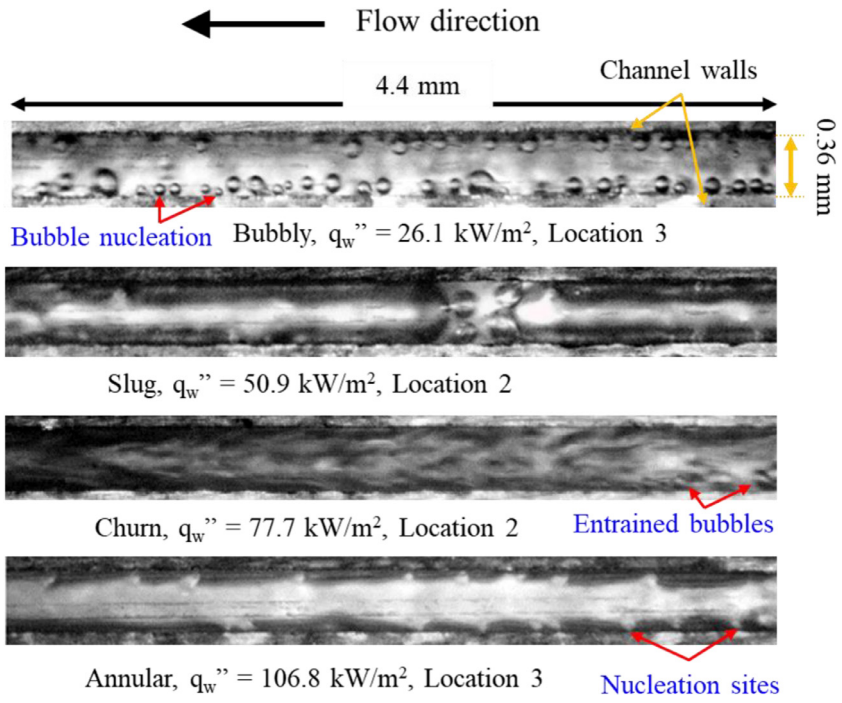

Fig. 5. Dominant flow patterns at increasing wall heat fluxes in the microchannels, see Fig. 2 for locations.

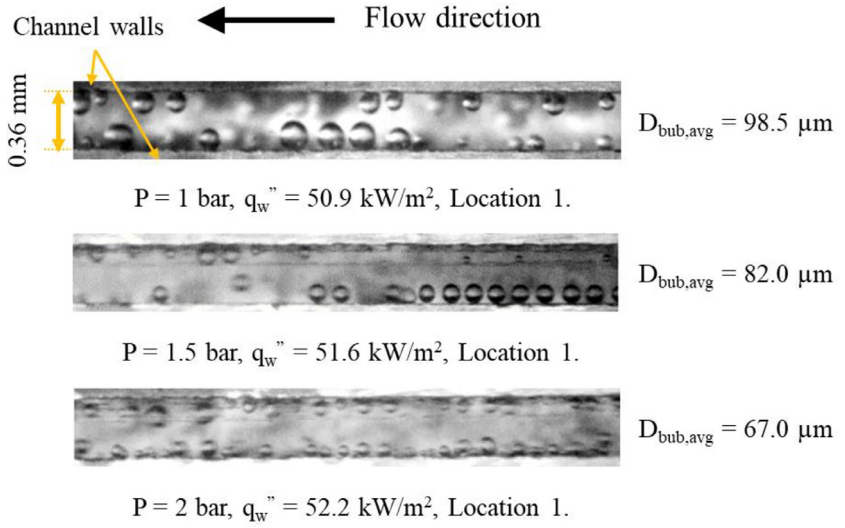

Fig. 6. Average bubble diameters in bubbly flow at different system pressures, captured at camera location 1 (near the channel inlet) at q_w" ~ 50 kW/m², see Fig. 2 for locations.

forces on bubbles at higher system pressures could also have contributed to smaller bubble departure diameters. Additionally, bubble departure diameter is intrinsically linked to bubble generation frequency, as reviewed in Situ et al. [16]. Although bubble generation frequency could not be independently verified in this study for a nominal cavity, the higher number of bubbles identified in the channels (see Fig. 7 to 9) could be an indication of higher bubble generation frequencies at larger operating pressures. The wider range of nucleation cavity sizes predicted using Hsu's model, as illustrated in Fig. 4, also supports this observation. With increase in system pressure, smaller nucleation sites, that is, if available on the surface of the boiling substrate, could have been activated, increasing the overall bubble generation rate in the channels.

There was some evidence suggesting an effect of pressure on liquid film thickness, and as a consequence the heat transfer rates with increase in system pressure. Due to limitations of the current visualisation set up (from the top of the channels), it was not possible to obtain an accurate measurement of the liquid film thickness and thus no conclusions are drawn in the current paper. Future investigations into the role of system pressure on liquid film thickness may be very useful for the understanding of microscale thin-liquid film evaporation.

3.3. Flow Instability

As covered above, Kuo and Peles [3,20] found that increasing the exit pressure from 50 kPa to 205 kPa mitigated flow oscillations due to rapid bubble growth of water microchannel flow boiling due to a reduction in boiling incipience wall superheat. Notably, there was a considerably larger influence of system pressure on the active nucleation range of water, as compared to the cur-

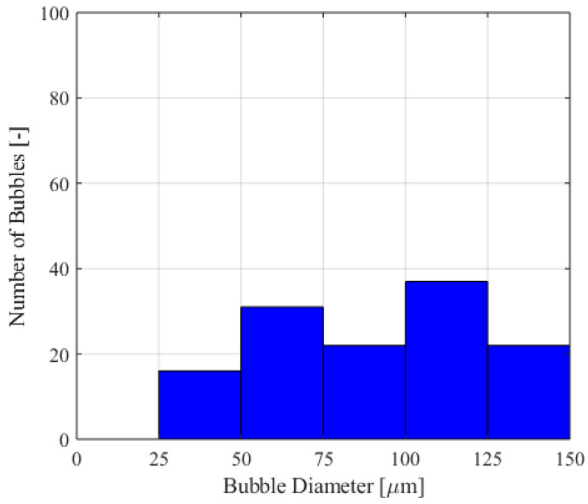

Fig. 7. Distribution of bubble diameters measured on five still frames of the high-speed recording at P = 1 bar, G = 200 kg/m^2 s, ΔT_{sub} = 10 K and $q_w^{"}$ = 50.9 kW/m^2.

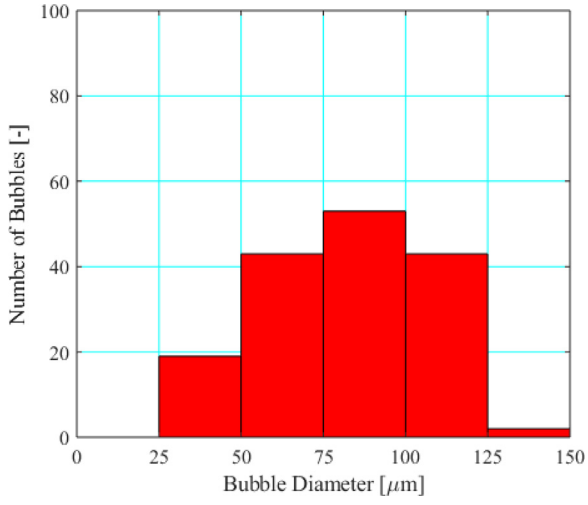

Fig. 8. Distribution of bubble diameters measured on five still frames of the high-speed recording at P = 1.5 bar, G = 200 kg/m^2 s, ΔT_{sub} = 10 K and $q_w^{"}$ = 51.6 kW/m^2.

rent range of pressures investigated for HFE-7200, see Fig. 4 for HFE-7200. It was unclear whether the degree of liquid inlet subcooling was kept constant in [3] and [20]. In the current study, the effect of system pressure is isolated from the effect of inlet subcooling as the degree of subcooling was maintained at ΔT_{sub} = 10 K.

Flow instabilities were typically observed in the slug flow regime in the current study at low wall heat fluxes near the onset of boiling in the heat sink, see section 3.2.3 in [32]. The measured pressure drop signal across the heat sink may be used to assess the extent of flow oscillations in the microchannels at different inlet pressures. The standard deviation of an experimental parameter, σ (Δj) , may be calculated as follows:

$$\sigma\left(\Delta j\right) = \sqrt{\frac{\sum_{n=1}^{n}\left(j_n - \overline{j_n}\right)^2}{n}} \tag{8}$$

where j represents the experimental parameter and n is the number of data points. In this case the variable j is the measured pressure drop value from the differential pressure transducer.

Kuo and Peles [3] used local transient temperature signals to study stages of unstable boiling in their silicon microchannel heat sink while researchers in [37–39] have also demonstrated the use of pressure and temperature signals to characterise the flow boiling instability phenomenon in microchannel heat sinks. In the present measurement setup, the response time of the 0.5 mm diameter K-type thermocouple used to measure fluid inlet temperature was specified by the manufacturer to be around 0.03 s [40]. As events such as bubble growth and coalescence in flow reversal occurs over a considerably shorter time period, as short as 16 ms, temperature measurement techniques with higher response rates should be employed. As the response time of the differential pressure transducer is less than 1 ms [41], based on manufacturer's specifications, the instrumentation to measure heat sink pressure drop is sufficient to capture flow oscillations due to vapour backflow in the current study.

Accordingly, the standard deviation of the measured pressure drop signal across the heat sink is presented in Fig. 10 for $q_w^{"} \sim$ 26 kW/m^2 in order to assess the effect of inlet pressure on flow boiling instabilities in the microchannel heat sink near the onset of boiling. The peaks and dips in the pressure drop signal may correspond to the occurrence of vapour backflow and recovery from flow reversal in the inlet plenum respectively, however it must be noted that flow visualisation was not conducted simultaneously with data recording in the current study. High speed recordings were only conducted when all readings on LabVIEW appear to be at steady-state condition for at least a window of 90 s and the flow phenomenon is observed to be quasi-steady. Hence, while the flow reversal phenomenon captured may not be directly linked to the pressure drop signals depicted in Fig. 10, it remains a good indication of the different stages of flow instability in the microchannel heat sink.

Increasing the operating pressure from P = 1 bar to P = 2 bar at the lowest wall heat flux condition (26 kW/m^2, corresponding to an exit vapour quality of x = 0.1) reduced pressure drop oscillations in the heat sink. The standard deviation in total pressure drop was 0.42 kPa at P = 1 bar, which reduced to 0.26 kPa and 0.17 kPa with pressure increment to P = 1.5 bar and P = 2 bar respectively. This is mainly because of the delay in flow regime transition to slug flow in the heat sink at higher pressures, as discussed extensively in Section 3.2, see Table 4. The delay in flow pattern transition may be attributed to smaller bubble diameters at higher pressures, as illustrated in Fig. 6. Similarly, Kuo and Peles [3] also found that increasing the operating pressure suppressed temperature oscillations at low vapour qualities of up to x = 0.15 due to lower wall superheat and smaller bubble departure diameters. The magnitude of temperature oscillations were almost 40 % lower at 205 kPa compared to at 101 kPa at a given vapour quality condition. Improving axial heat conduction in the channel walls could also reduce the amplitude of temperature and pressure oscillations, as reported in [12].

3.4. Heat Transfer

The effect of inlet pressure on the average two-phase heat transfer coefficient at a fixed mass flux of G = 200 kg/m^2 s and inlet subcooling of ΔT_{sub} = 10 K for wall heat fluxes in the range of $q_w^{"}$ = 26.3 – 164.2 kW/m^2 may be inferred from Fig. 11.

With inlet pressure increase from 1 bar to 1.5 bar, there is a slight increase in the heat transfer coefficient across the range of heat fluxes investigated, except at the lowest heat flux level ($q_w^{"} \sim$ 26 kW/m^2). The pressure effect is less significant between operating pressures 1.5 bar and 2 bar at low heat fluxes, but begin to diverge slightly toward high heat fluxes ($q_w^{"} \sim$ 134 – 157 kW/m^2). In fact, at low heat fluxes ($q_w^{"} \sim$ 26 kW/m^2 and $q_w^{"} \sim$ 50 kW/m^2), increasing inlet pressure from 1.5 bar to 2 bar did not ap-

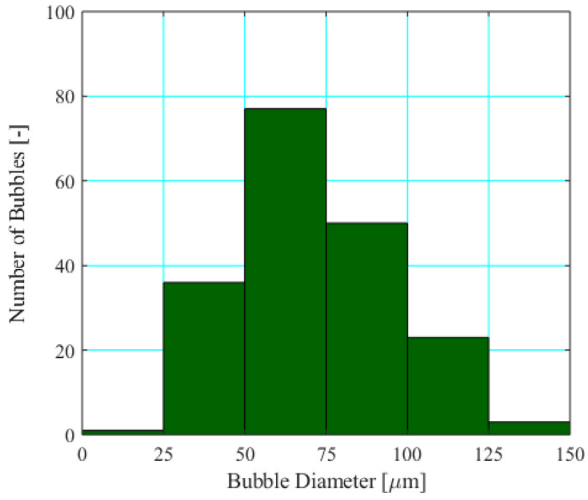

Fig. 9. Distribution of bubble diameters measured on five still frames of the high-speed recording at P = 2 bar, G = 200 kg/m^2 s, ΔT_{sub} = 10 K and $q_w^{"}$ = 52.2 kW/m^2.

pear to have an effect on the heat transfer coefficient in the channels. Fig. 12 shows the local heat transfer coefficients with respect to streamwise location at $q_w^{"} \sim 51$ kW/m^2. The subcooled and saturated region are annotated on the graph. Heat transfer coefficients in the subcooled region exhibited a similar pressure effect to that found in the flow boiling region. Fig. 13 and Fig. 14 clearly depict a more pronounced pressure effect on the heat transfer coefficient at moderate and high heat fluxes ($q_w^{"} \sim 110$ kW/m^2 and $q_w^{"} \sim 160$ kW/m^2 respectively).

In the low heat flux region, $q_w^{"} \sim 26 - 50$ kW/m^2, bubbly flow dominated over at least half the channel length, implying that nucleate boiling was dominant at these conditions. Hence the heat transfer enhancement at low heat fluxes could be due to an increase in bubble generation frequency with increase in inlet pressure. This is explained above using Hsu's model (see Fig. 4), and is also supported by our flow visualisation results, where a larger number of bubbles were identified at higher operating pressures as evident in Fig. 7 to Fig. 9.

The reduced pressure, P_r, is an important parameter in the estimation of the nucleate boiling heat transfer coefficient, for instance in Cooper's correlation [42], where boiling heat transfer coefficient in the nucleate regime, h_{nb}, is directly correlated to reduced pressure, surface roughness and molecular weight (see Eq. (9)).

$$h_{nb} = 55\, P_r^{0.12 - 0.434 \ln Rp} \left(-\log P_r\right)^{-0.55} M^{-0.5}\, q^{0.67} \quad (9)$$

Note that the roughness parameter in the correlation, Rp, is in units of μm.

The reduced pressure ratio doubled between P = 1 bar and P = 1.5 bar. At a wall heat flux of $q_w^{"}$ = 50 kW/m^2, Cooper's correlation predicts an increase in h_{nb} from 1399 W/m^2 K to 1753 W/m^2 K, i.e. by 25.3 % between these conditions. Other than that, the change in fluid properties, namely vapour density and surface tension could also have played a role in the enhancing two-phase heat transfer at higher system pressures. Vapour density increased by almost 50 % while surface tension fell by 12.5 % corresponding to pressure increase from P = 1 bar to P = 1.5 bar. Karayiannis et al. [30] and Xu et al. [23] suggested that a reduction in surface tension is beneficial to flow boiling heat transfer.

Interestingly, at heat flux levels $q_w^{"} \sim 26$ kW/m^2 and $q_w^{"} \sim 50$ kW/m^2, no significant enhancement in heat transfer between P = 1.5 bar and P = 2 bar was recorded. This is clearly illustrated in Fig. 12. Incidentally, flow pattern transition boundaries differed much less between these pressures (see Table 4, $x_{B\text{-}S}$). In Fig. 4, the size range of nucleation sizes were only weakly dependent on pressure at low wall superheat levels.

At moderate and high heat fluxes, churn and annular flow tended to dominate the flow pattern in the channels. Alongside nucleate boiling, the convective boiling mechanism also begins to dominate in these flow regimes due to liquid film evaporation from the heated channel walls. The pressure effect between P = 1 bar and P = 1.5 bar remained constant, whilst a stronger pressure effect, previously weak at low heat fluxes (see Fig. 12), manifests between P = 1.5 bar and P = 2 bar, see Fig. 11. This observation is in contradiction with the conclusion reported by Wen et al. [29] and In and Jeong [31], where insignificant inlet pressure effects on heat transfer coefficient were found at high vapour qualities where convective boiling were assumed to dominate. These studies were for minichannels and microtubes. However, in the current study, a drop in average heat transfer coefficient was not recorded in the channels, even at high vapour qualities. This may be because nucleate boiling is seen to still be active in annular flow, as reported in a related study [43].

The pressure effect in this study was only conducted at one mass flux, i.e. 200 kg/m^{2}s. However at a fixed inlet pressure of 1 bar, a mass flux study at 200, 300 and 400 kg/m^{2}s was conducted. At higher mass flux, the vapour quality range where bubbly and slug was observed is narrowed, thus the pressure effect observed in these two regimes will be less prevalent at higher mass fluxes. The dominant pressure effect observed is postulated in the churn and annular region, where its effects on liquid film thickness (and by extension, the heat transfer rates) is suggested for further investigation.

The effect of pressure in the heat flux region where thin-film evaporation dominates could be understood by applying the three-zone model proposed by Thome et al. [44], which was more recently modified by Magnini and Thome [45]. As the three-zone model relies heavily on the liquid film thickness in the heat transfer coefficient predictions, high-fidelity measurements of the film thicknesses are required. With the updated model applying the Moriyama and Inoue [46] correlation, it can however be shown that liquid film thickness decreased with respect to increasing bubble generation frequency.

3.5. Pressure Drop

The effect of system pressure on two-phase pressure drop in the channels is shown in Fig. 15 as a function of wall heat flux. Increasing the inlet pressure reduced the two-phase pressure drop across the microchannel heat sink, although a weaker pressure effect is observed between system pressures P = 1.5 bar and P = 2 bar. The deviation in pressure drop with system pressure is likely unrelated to flow pattern development in the channels. As reported above, flow patterns developed accordingly across all inlet pressures, with a small delay in flow pattern transition vapour qualities at higher pressures. A reduction in two-phase pressure drop in response to system pressure increase was also reported by Kuo and Peles [3], Saisorn et al. [4] and Dário et al. [5].

As highlighted above, frictional pressure loss and acceleration pressure loss are dependent on fluid properties, such as density and viscosity, which have been shown to vary significantly with pressure changes in Table 2 and 3. In fact, the effect of pressure can be observed in the slip ratio, two-phase multiplier as well as the Martinelli parameter when estimating two-phase frictional pressure drop. With increase in system pressure, all the above-mentioned parameters decreased considerably due to changes in the physical properties of the fluid. The resultant frictional pressure drop and gravitational pressure drop components, as predicted based on the Lockhart-Martinelli correlation [47] for the operating pressures investigated, are shown in Fig. 16 and Fig. 17 re-

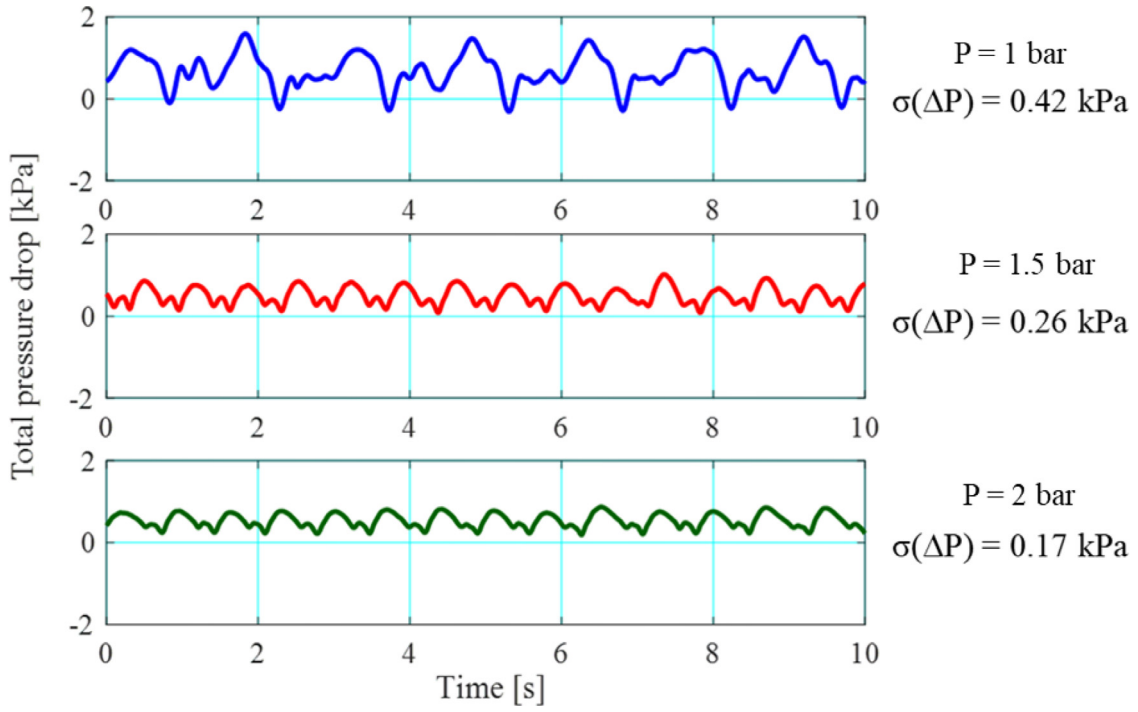

Fig. 10. Measured pressure drop across the heat sink at $q_w^{"} \sim 26$ kW/m^2 over a window of 20 s for G = 200 kg/m^2 s and ΔT_{sub} = 10 K at system pressures 1 bar to 2 bar.

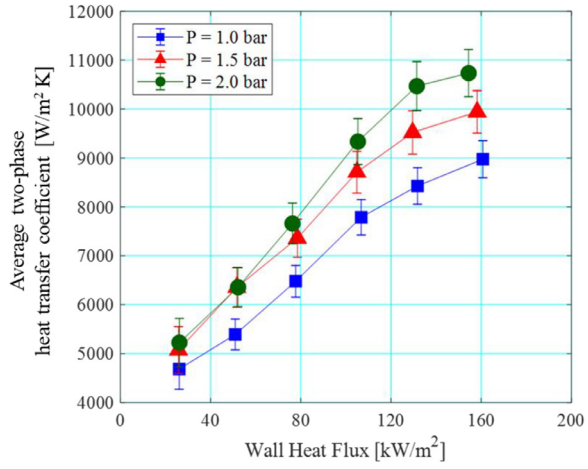

Fig. 11. Average two-phase heat transfer coefficients with respect to wall heat flux ($q_w^{"}$ = 26.1 – 160.7 kW/m^2), at G = 200 kg/m^2 s and ΔT_{sub} = 10 K for three inlet pressure conditions.

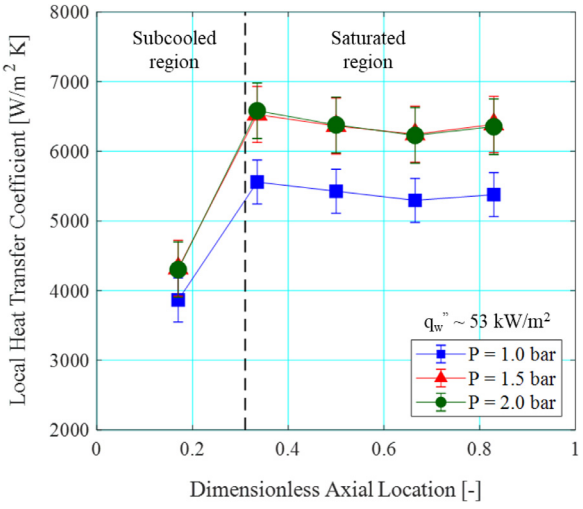

Fig. 12. Local heat transfer coefficients as a function of streamwise location on the channels, at G = 200 kg/m^2 s, ΔT_{sub} = 10 K and $q_w^{"} \sim 50$ kW/m^2 .

spectively. These are based on the following equations [6]:

$$\Delta P_{fric} = \frac{2\, f_{fo}\, G^2\, \nu_f\, L_{tp}}{D_h}\left[\frac{1}{x}\int_0^x \phi_{fo}^2 dx\right] \quad (10)$$

$$\Delta P_{acc} = G^2\, \nu_f \left[\frac{x^2}{\alpha_v}\frac{\rho_f}{\rho_g} + \frac{(1-x)^2}{(1-\alpha_v)} - 1\right] \quad (11)$$

Note that these are predicted to depict the trend in component pressure drop but do not reflect the experimental pressure drop values. Frictional pressure drop decreased with increase in pressure, especially between P = 1 bar and P = 1.5 bar, while a weaker pressure effect was observed between P = 1.5 bar and P = 2 bar. A similar trend was found for the acceleration pressure drop component.

As established above, frictional pressure loss is largely influenced by the magnitude of the two-phase multiplier. It was mentioned earlier that a large rise in vapour density of up to 47.5 % was registered with system pressure increase from P = 1 bar to P = 1.5 bar. This resulted in a notable rise in the vapour to liquid density ratio, ($\frac{\rho_g}{\rho_f}$), namely by 51.7 %. For a given vapour quality condition, the two-phase multiplier ϕ_{fo}^2 decreased with increasing system pressure, lowering the frictional pressure loss in the system. Other than that, liquid viscosity, μ_f, decreased by 13.9 % while gas viscosity, μ_g, rose by 8.3 % corresponding to inlet pressure increase from P = 1 bar to P = 1.5 bar. The respective changes in viscosity affect the Reynolds number of the liquid as well as gas flow, and by extension the Darcy friction factor of the liquid and gas phase, i.e. f_{fo} = 64/Re in the laminar regime. Nonetheless, only a moderate drop in liquid-vapour friction factor ratio of 15.8 % occurred between P = 1 bar and P = 1.5 bar. The reduction in ϕ_{fo}^2 and frictional pressure drop was mainly governed by the change

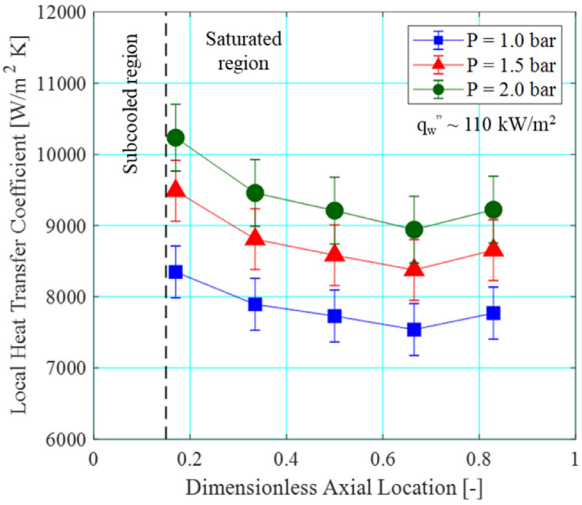

Fig. 13. Local heat transfer coefficients as a function of streamwise location on the channels, at G = 200 kg/m² s, ΔT_{sub} = 10 K and $q_w^{"}$ ~ 110 kW/m² .

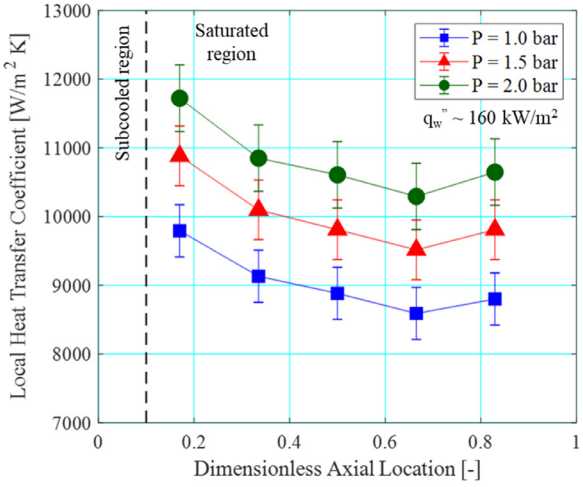

Fig. 14. Local heat transfer coefficients as a function of streamwise location on the channels, at G = 200 kg/m² s, ΔT_{sub} = 10 K and $q_w^{"}$ ~ 160 kW/m².

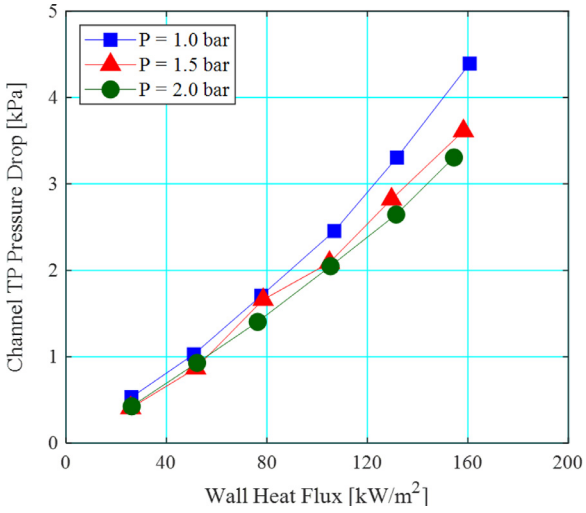

Fig. 15. Two-phase pressure drop in the channels with respect to wall heat flux at G = 200 kg/m² s and ΔT_{sub} = 10 K for three inlet pressure conditions.

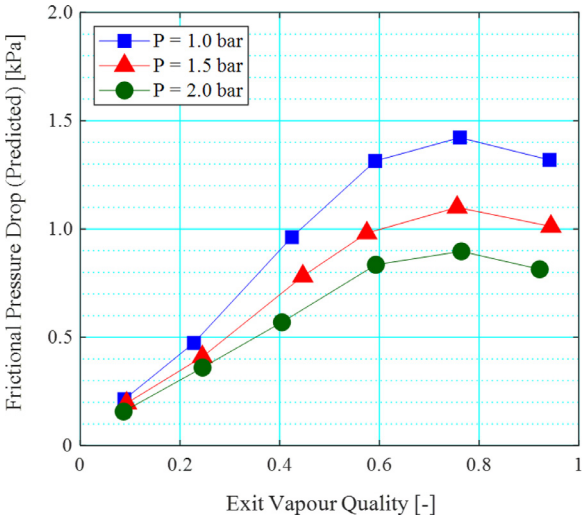

Fig. 16. The two-phase frictional pressure drop component with respect to exit quality, estimated using the Lockhart-Martinelli correlation [47] for G = 200 kg/m² s and ΔT_{sub} = 10 K.

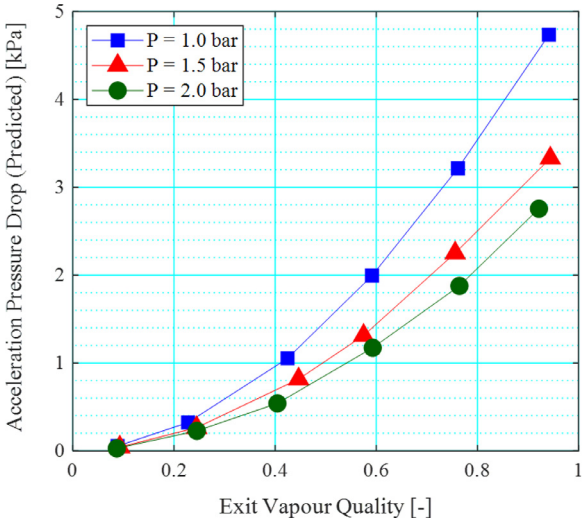

Fig. 17. The two-phase acceleration pressure drop component with respect to exit quality, estimated using the Lockhart-Martinelli correlation [47] for G = 200 kg/m² s and ΔT_{sub} = 10 K.

in vapour-liquid density ratio, in direct relation to the increase in system pressure for a given heat flux and vapour quality condition in the heat sink.

The weaker pressure effect between P = 1.5 bar and P = 2 bar could be due to the comparatively smaller increase in vapour density between pressures of 1.5 bar and 2 bar. (32.9 % compared to 47.4 % at the lower pressure). This brought about a milder increase in density ratio in the fluid (26.1 % compared to 34 % at the lower pressure), which slightly narrowed the disparity ϕ_{fo}^2 for a given vapour quality between P = 1.5 bar and P = 2 bar. Consequently, a smaller deviation in frictional pressure drop trend is observed between these pressures in Fig. 16.

The model also predicted a drop in the two-phase acceleration pressure drop with increase in system pressure in the system, see Fig. 17. Evident from Eq. (11), the acceleration pressure drop is directly related to the liquid-to-vapour density ratio, $(\frac{\rho_f}{\rho_g})$, of the fluid. As noted above, liquid density remains largely unaltered across the pressure range studied while the vapour density increased by nearly 50 % at the lower pressure increase and by

just over 30 % with further increase in operating pressure to 2 bar. ($\frac{\rho_f}{\rho_g}$) decreased by 34 % and 26.1 % accordingly. As a direct consequence, the acceleration pressure drop decreased with increasing inlet pressure for a given heat flux and vapour quality condition. The smaller pressure effect observed between P = 1.5 bar and P = 2 bar, as concluded above, could be due to the smaller corresponding increase in vapour density, which produced a smaller decrease in ($\frac{\rho_f}{\rho_g}$) of only 26.1 % between these pressures. Whilst the notable change in vapour density also affects the void fraction, the ultimate decrease in α_v was insignificant, owing to the small range as well as magnitude of α_v (i.e. >>1 when x > 0.2 in the present study).

4. Conclusions

The effect of system pressure, i.e. 1.0, 1.5 and 2.0 bar, on the flow boiling characteristics of HFE-7200 was investigated in isolation to all other experimental parameters, i.e. at a mass flux of 200 kg/m^2 s and subcooling degree of 10 K in a parallel microchannel heat sink (D_h = 0.48 mm) at heat fluxes between 26.1 – 160.7 kW/m^2. Flow visualisation, heat transfer and pressure drop data were presented. The experiments demonstrated that that modifying the operating pressure could be a viable way to manage flow instabilities in two-phase microchannel systems using HFE-7200, without significant heat sink design effort and pressure drop penalty, along with advantages in heat transfer rates.

In the range of the present study, increasing system pressure decreased the vapour density drastically, thus reducing the liquid-vapour density dimensionless ratio. Increasing inlet pressure reduced surface tension. A smaller variation in fluid properties was observed between 1.5 bar and 2 bar. For HFE-7200, there was a negligible pressure effect on nucleation cavity size (< 2K) but smaller cavity sizes become activated with increasing pressure at higher superheats.

A similar flow regime development was observed in the microchannel array at all pressures investigated, i.e. bubbly-slug-churn-annular flow. There was however a general decrease in flow pattern transition vapour quality, attributed to smaller bubble diameters found at higher operating pressures. It can be inferred from the number of bubbles present that the bubble nucleation frequency increased with pressure. This was postulated to be related to the vapour density variation with pressure, liquid-to-vapour density ratio and secondarily to surface tension. The delay in flow regime transition to slug flow, a regime prone to flow reversal, was also demonstrated to reduce pressure drop oscillations at higher operating pressures in the microchannel heat sink.

In general, increasing inlet pressure increased the flow boiling heat transfer coefficient in the microchannel heat sink. This was attributed to higher bubble generation frequency, as observed in the flow visualisation experiments and is mostly due to changes in fluid properties. This was demonstrated though an increase in the reduced pressure ratio and lower surface tension with increasing inlet pressure. There was a negligible effect at the two higher pressures under low heat flux conditions, which may be due to low wall superheat (small difference in nucleation size range) and smaller variation in fluid properties at these conditions.

Relatively low magnitudes of pressure drop were measured in the current study. Nonetheless, a small decrease in two-phase pressure drop was observed with increments in system pressure. This was related to the variation in fluid properties, mainly a reduction in vapour density and liquid-to-vapour density ratio, thus resulting in lower two-phase pressure drop in the microchannels.

Author Statement

T. G. Karayiannis planned the project. V.Y.S. Lee designed and constructed the test section and commissioned the experimental facility under the supervision of T.G. Karayiannis. V.Y.S. Lee carried out the experiments and presented the results and first draft for changes and additions to T.G. Karayiannis. Both authors discussed the results and contributed to the final manuscript.

Declaration of Competing Interest

The authors declare that they have no known competing financial interests or personal relationships that could have appeared to influence the work reported in this paper.

Data availability

Data will be made available on request.

Acknowledgements

The authors would like to acknowledge the support of CPI TMD Technologies Division (formerly TMD Technologies Ltd.) and Mr Costas Xanthos of the Two-Phase Flow and Heat Transfer Group at Brunel University London for this work.

References

[1] Y.Y. Hsu, On the size range of active nucleation cavities on a heating surface, J. Heat Transfer 84 (3) (1962) 207–213, doi:10.1115/1.3684339.
[2] M.M. Mahmoud, T.G. Karayiannis, Flow Boiling in Mini to Microdiameter Channels, in: J.R. Thome (Ed.), Encyclopedia of Two-Phase Heat Transfer and Flow IV, World Scientific Publishing, 2018, pp. 233–301, doi:10.1142/9789813234444_0004.
[3] C.-J. Kuo, Y. Peles, Pressure effects on flow boiling instabilities in parallel microchannels, Int. J. Heat Mass Transf. 52 (1–2) (2009) 271–280, doi:10.1016/J.IJHEATMASSTRANSFER.2008.06.015.
[4] S. Saisorn, J. Kaew-On, S. Wongwises, Flow pattern and heat transfer characteristics of R-134a refrigerant during flow boiling in a horizontal circular mini-channel, Int. J. Heat Mass Transf. 53 (19–20) (Sep. 2010) 4023–4038, doi:10.1016/J.IJHEATMASSTRANSFER.2010.05.022.
[5] E.R. Dário, J.C. Passos, M.L. Sánchez Simón, L. Tadrist, Pressure drop during flow boiling inside parallel microchannels, Int. J. Refrig. (2016), doi:10.1016/j.ijrefrig.2016.08.002.
[6] J.G. Collier, J.R. Thome, *Convective Boiling and Condensation*, Third, Clarendon Press, 1996.
[7] F.P. Incropera, T.L. Bergman, D.P. DeWitt, A.S. Lavine, Fundamentals of Heat and Mass Transfer, 7th Edition, John Wiley & Sons, 2012, doi:10.1016/j.applthermaleng.2011.03.022.
[8] S.S. Kutateladze, "On the transition to film boiling under natural convection," *Kotloturbostroenie*, vol. 3, pp. 10–12, 1948, Accessed: Jan. 23, 2022. [Online]. Available: https://ci.nii.ac.jp/naid/10027011442
[9] N. Zuber, On Stability of Boiling Heat Transfer, Trans. ASME 80 (1958) 711–720 Accessed: Jan. 23, 2022. [Online]. Available https://www.osti.gov/biblio/4326542 .
[10] J.H. Lim, M. Park, Flow Boiling Burnout in a Hypervapotron Channel Under High Heat Flux and High Sub-Cooling Conditions, J. Fusion Energy 41 (1) (Jun. 2022) 1–12, doi:10.1007/S10894-022-00316-W/FIGURES/9.
[11] T. Zhang, et al., Ledinegg instability in microchannels, Int. J. Heat Mass Transf. 52 (Dec. 2009) 25–26 5661–5674Accessed: Jun. 09, 2019. [Online]. Available https://linkinghub.elsevier.com/retrieve/pii/S001793100900489X .
[12] G. Xia, Y. Lv, L. Cheng, D. Ma, Y. Jia, Experimental study and dynamic simulation of the continuous two-phase instable boiling in multiple parallel microchannels, Int. J. Heat Mass Transf. 138 (2019) 961–984, doi:10.1016/j.ijheatmasstransfer.2019.04.124.
[13] G. Liang, I. Mudawar, Review of channel flow boiling enhancement by surface modification, and instability suppression schemes, Int. J. Heat Mass Transf. 146 (Jan. 2020) 118864, doi:10.1016/J.IJHEATMASSTRANSFER.2019.118864.
[14] D. Euh, B. Ozar, T. Hibiki, M. Ishii, C.-H. Song, Characteristics of Bubble Departure Frequency in a Low-Pressure Subcooled Boiling Flow, J. Nucl. Sci. Technol. 47 (7) (2010) 608–617, doi:10.1080/18811248.2010.9720958.
[15] S.M.S. Murshed, K. Vereen, D. Strayer, R. Kumar, An experimental investigation of bubble nucleation of a refrigerant in pressurized boiling flows, Energy 35 (12) (Dec. 2010) 5143–5150, doi:10.1016/J.ENERGY.2010.07.052.
[16] R. Situ, M. Ishii, T. Hibiki, J.Y.Y. Tu, G.H.H. Yeoh, M. Mori, Bubble departure frequency in forced convective subcooled boiling flow, Int. J. Heat Mass Transf. 51 (25–26) (Dec. 2008) 6268–6282, doi:10.1016/j.ijheatmasstransfer.2008.04.028.

[17] J.F. Klausner, R. Mei, D.M. Bernhard, L.Z. Zeng, Vapor bubble departure in forced convection boiling, Int. J. Heat Mass Transf. 36 (3) (1993) 651–662, doi:10.1016/0017-9310(93)80041-R.
[18] V. Prodanovic, D. Fraser, M. Salcudean, Bubble behavior in subcooled flow boiling of water at low pressures and low flow rates, Int. J. Multiph. Flow 28 (1) (Jan. 2002) 1–19, doi:10.1016/S0301-9322(01)00058-1.
[19] D. Yuan, L. Pan, D. Chen, H. Zhang, J. Wei, Y. Huang, Bubble behavior of high subcooling flow boiling at different system pressure in vertical narrow channel, Appl. Therm. Eng. 31 (16) (Nov. 2011) 3512–3520, doi:10.1016/J.APPLTHERMALENG.2011.07.004.
[20] C.-J.J. Kuo, Y. Peles, Flow Boiling Instabilities in Microchannels and Means for Mitigation by Reentrant Cavities, J. Heat Transfer 130 (7) (Jul. 2008), doi:10.1115/1.2908431.
[21] I. Mudawar, M.B. Bowers, Ultra-high critical heat flux (CHF) for subcooled water flow boiling—I: CHF data and parametric effects for small diameter tubes, Int. J. Heat Mass Transf. 42 (8) (1999) 1405–1428, doi:10.1016/S0017-9310(98)00241-5.
[22] X. Huo, L. Chen, Y.S. Tian, T.G. Karayiannis, Flow boiling and flow regimes in small diameter tubes, Appl. Therm. Eng. 24 (8–9) (2004) 1225–1239, doi:10.1016/J.APPLTHERMALENG.2003.11.027.
[23] Y. Xu, X. Fang, G. Li, D. Li, Y. Yuan, An experimental study of flow boiling heat transfer of R134a and evaluation of existing correlations, Int. J. Heat Mass Transf. 92 (2016) 1143–1157, doi:10.1016/J.IJHEATMASSTRANSFER.2015.09.044.
[24] B. Agostini, J.R. Thome, M. Fabbri, B. Michel, D. Calmi, U. Kloter, High heat flux flow boiling in silicon multi-microchannels – Part II: Heat transfer characteristics of refrigerant R245fa, Int. J. Heat Mass Transf. 51 (21–22) (Oct. 2008) 5415–5425, doi:10.1016/J.IJHEATMASSTRANSFER.2008.03.007.
[25] S. Basu, et al., Flow Boiling of R134a in Circular Microtubes—Part I: Study of Heat Transfer Characteristics, J. Heat Transfer 133 (5) (2011) 051502, doi:10.1115/1.4003159.
[26] S.S. Bertsch, E.A. Groll, S.V. Garimella, Refrigerant flow boiling heat transfer in parallel microchannels as a function of local vapor quality, Int. J. Heat Mass Transf. 51 (19–20) (Sep. 2008) 4775–4787, doi:10.1016/J.IJHEATMASSTRANSFER.2008.01.026.
[27] S.S. Bertsch, E.A. Groll, S.V. Garimella, Effects of heat flux, mass flux, vapor quality, and saturation temperature on flow boiling heat transfer in microchannels, Int. J. Multiph. Flow 35 (2) (2009) 142–154, doi:10.1016/J.IJMULTIPHASEFLOW.2008.10.004.
[28] P. Thiangtham, et al., An experimental study on two-phase flow patterns and heat transfer characteristics during boiling of R134a flowing through a multi-microchannel heat sink, Int. J. Heat Mass Transf. 98 (2016) 390–400, doi:10.1016/J.IJHEATMASSTRANSFER.2016.02.051.
[29] T. Wen, H. Zhan, D. Zhang, Flow boiling heat transfer in mini channel with serrated fins: Experimental investigation and development of new correlation, Int. J. Heat Mass Transf. 128 (May 2017) 1081–1094 2019, doi:10.1016/j.ijheatmasstransfer.2018.09.071.
[30] T.G. Karayiannis, M.M. Mahmoud, D.B.R. Kenning, A study of discrepancies in flow boiling results in small to microdiameter metallic tubes, Exp. Therm. Fluid Sci. 36 (Jan. 2012) 126–142, doi:10.1016/J.EXPTHERMFLUSCI.2011.09.005.
[31] S. In, S. Jeong, Flow boiling heat transfer characteristics of R123 and R134a in a micro-channel, Int. J. Multiph. Flow 35 (11) (2009) 987–1000, doi:10.1016/J.IJMULTIPHASEFLOW.2009.07.003.
[32] V.Y.S. Lee, T.G. Karayiannis, Effect of inlet subcooling on flow boiling in microchannels, Appl. Therm. Eng. 181 (Nov. 2020) 115966, doi:10.1016/j.applthermaleng.2020.115966.
[33] W. Hugh, W.Glenn Coleman, Steele, *Experimentation, Validation, and Uncertainty Analysis for Engineers*, 3rd Edition, John Wiley & Sons, 2009.
[34] N. Zuber, The dynamics of vapor bubbles in nonuniform temperature fields, Int. J. Heat Mass Transf. 2 (1–2) (1961) 83–98, doi:10.1016/0017-9310(61)90016-3.
[35] B.B. Mikic, W.M. Rohsenow, P. Griffith, On bubble growth rates, Int. J. Heat Mass Transf. 13 (1970) 657–666, doi:10.1016/0017-9310(70)90040-2.
[36] P.C. Lee, F.G. Tseng, C. Pan, Bubble dynamics in microchannels. Part I: single microchannel, Int. J. Heat Mass Transf. 47 (25) (2004) 5575–5589, doi:10.1016/J.IJHEATMASSTRANSFER.2004.02.031.
[37] D. Bogojevic, K. Sefiane, A.J. Walton, H. Lin, G. Cummins, Two-phase flow instabilities in a silicon microchannels heat sink, Int. J. Heat Fluid Flow 30 (2009) 854–867, doi:10.1016/j.ijheatfluidflow.2009.03.013.
[38] T.A. Kingston, J.A. Weibel, S.V. Garimella, High-frequency thermal-fluidic characterization of dynamic microchannel flow boiling instabilities: Part 2 – Impact of operating conditions on instability type and severity, Int. J. Multiph. Flow 106 (Sep. 2018) 189–201, doi:10.1016/J.IJMULTIPHASEFLOW.2018.05.001.
[39] T.A. Kingston, J.A. Weibel, S.V. Garimella, Time-resolved characterization of microchannel flow boiling during transient heating: Part 1 – Dynamic response to a single heat flux pulse, Int. J. Heat Mass Transf. 154 (Jun. 2020) 119643, doi:10.1016/j.ijheatmasstransfer.2020.119643.
[40] TC Ltd, "Mineral Insulated Thermocouples - Type 12," 2019. Accessed: Apr. 20, 2020. [Online]. Available: www.tc.co.uk
[41] Omega Engineering, "Micro-Machined Silicon Wet/Wet Differential Pressure Transducers." https://www.omega.co.uk/pptst/PX409-WWDIF.html (accessed Apr. 20, 2020).
[42] M.G.G. Cooper, Heat Flow Rates in Saturated Nucleate Pool Boiling-A Wide-Ranging Examination Using Reduced Properties, Adv. Heat Transf. 16 (Jan. 1984) 157–239 no. C, doi:10.1016/S0065-2717(08)70205-3.
[43] V.Y.S. Lee, G. Henderson, A. Reip, T.G. Karayiannis, Flow boiling characteristics in plain and porous coated microchannel heat sinks, Int. J. Heat Mass Transf. 183 (Feb. 2022) 122152, doi:10.1016/j.ijheatmasstransfer.2021.122152.
[44] J.R. Thome, V. Dupont, A.M. Jacobi, Heat transfer model for evaporation in microchannels. Part I: Presentation of the model, Int. J. Heat Mass Transf. (2004), doi:10.1016/j.ijheatmasstransfer.2004.01.006.
[45] M. Magnini, J.R. Thome, An updated three-zone heat transfer model for slug flow boiling in microchannels, Int. J. Multiph. Flow (2017), doi:10.1016/j.ijmultiphaseflow.2017.01.015.
[46] K. Moriyama, A. Inoue, Thickness of the liquid film formed by a growing bubble in a narrow gap between two horizontal plates, J. Heat Transfer 118 (1) (Feb. 1996) 132–139, doi:10.1115/1.2824026.
[47] R.W. Lockhart, R.C. Martinelli, Proposed correlation of data for isothermal two-phase, two-component flow in pipes, Chem. Engng Prog. 45 (1) (1949) 39–48.